# Grid-Friendly Matching of Synchronous Machines by Tapping into the DC Storage ⋆

**Taouba Jouini** * **Catalin Arghir** * **Florian Dörfler** *

* *Automatic Control Laboratory at ETH Zürich, Switzerland (e-mail: tjouini@student.ethz.ch, carghir@control.ee.ethz.ch, dorfler@ethz.ch)*

**Abstract:** We propose a novel control strategy for grid-forming converters in low-inertia power grids. Our strategy is inspired by identifying the structural similarities between the 3-phase DC/AC converter and the synchronous machine model. We explicitly match these models through modulation control so that they become structurally equivalent. Compared to standard emulation of virtual synchronous machines, our controller relies solely on readily available DC-side measurements and takes into account the natural DC and AC storage elements which are usually neglected. As a result, our controller is generally faster and less vulnerable to delays and measurement inaccuracies. We provide a virtual adaptive oscillator interpretation of our controller various plug-and-play properties of the closed loop, such as passivity with respect to the DC and AC ports as well as the steady-state droop slopes, which we illustrate in simulations.

## 1. INTRODUCTION

Power systems are increasingly based on non-rotational generation with power electronic converters interfacing renewables and batteries with the AC power grid. A major challenge in such low-inertia networks is the replacement of the stabilizing rotational inertia of synchronous machines (SMs) and their ancillary services through control of converters (Tielens and Van Hertem, 2016). These so-called *grid-forming* converter control strategies range from the emulation of virtual synchronous machines (VSMs) and their controls to more general oscillator-based strategies. VSMs in particular are often brand-marked as *grid-friendly* since they are based on fully decentralized control, naturally backward compatible with SMs, and ultimately increase the system inertia (Vasileios Karapanos, 2011).

All implementations of VSMs known to us, rely on encoding a SM model on an embedded micro-controller that is fed by AC measurements at the converter terminals. The outputs of the SM model again provide references for the converter currents and voltages that are tracked through cascaded inner loops and ultimately result in gate signals for the converter (D'Arco and Suul, 2013; Yong Chen and Beck, 2011; Zhong and Weiss, 2011). Different challenges arise depending on the particular VSM implementation. The usage of phase-locked-loops to generate frequency references for the VSM results in a high dependence on real-time AC frequency measurements (Vasileios Karapanos, 2011; M.P.N van Wesenbeeck and Visscher, 2009), and any frequency tracking errors severely affect the control performance (D'Arco and Suul, 2013). Also delays in the acquisition and processing of AC measurements (e.g., averaging over multiple cycles) degrade the performance (Bevrani et al., 2014). Moreover, VSM implementations also crucially depend on the fidelity and accuracy of the mathematical SM model (encoded in software): e.g., VSM emulations range from (rather inaccurate) swing equation models to highly detailed multi-axis generator models that give rise to very different closed-loop behavior. Finally, *smarter* control actions are needed other than mere VSM emulation when the power system has a significant share of power electronic generation (Tielens and Van Hertem, 2016) since, among others, the time-delays of VSM emulation can result in system failures (ENTSOE, 2016), and VSM can tolerate considerably smaller short-circuit currents than SMs (Denis et al., 2015). One solution is of course to use the analog storage available on the DC-side of a converter. (Arani and El-Saadany, 2013) provides an interesting perspective: namely, the super-capacitor connected to the DC-link mimics the mass behavior of SM and outperforms virtual inertia emulation.

In this paper we propose an alternative control that uses the natural storage elements of a converter, in particular, the DC capacitor as in (Arani and El-Saadany, 2013), and that takes into account the difficulties of VSM emulation, such as delays and inaccuracies incurred by AC measurements (Vasileios Karapanos, 2011). Rather than merely emulating a SM, our control strategy is inspired by the structural similarities between a higher-order SM model and an averaged converter model. We *match* the two models by designing an appropriate modulation control. We analyze the passivity properties of the closed loop with respect to the DC and AC ports, as well as the steady-state power injection profile and droop slopes. We thus establish all plug-and-play properties required by a grid-forming source, which we confirm with detailed simulations. The equivalence of our closed-loop to a SM is only structural due to the different sizing of the storage elements. This sizing offers flexibility in tuning the matching control and adding outer loops, e.g., virtual governor, PSS, or inertia.

Compared to VSM emulation, our matching control has the following advantages: it relies on a DC voltage measurement, it does not require a mathematical SM model on a micro-controller or any inner tracking control loops,

⋆ This research is supported by ETH funds and the SNF Assistant Professor Energy Grant #160573.

and it naturally and explicitly integrates both AC and DC storage elements. Thus, it encounters shorter delays and inaccuracies in measurement acquisition, signal processing, and actuation than VSM. Our method can also be interpreted as oscillator-based controller similar to *virtual oscillator control* (VOC) (Johnson et al., 2014; Sinha et al., 2015) or *proportional resonant control* (PRC) (Teodorescu et al., 2006) and may strike a bridge between different grid-forming control strategies. Finally, our matching control provides a robust inner loop around which outer control loops can be added to regulate frequency and voltage.

The remainder of this paper is organized as follows, Section 2 presents the SM and the DC/AC converter model, and it proposes an intuitive control strategy to match them. Section 3 deals with the properties of the closed-loop DC/AC converter and highlights the plug-and-play characteristics of the converter at steady state. In Section 4, analytical solutions are confirmed with simulations after connecting the converter to a grid of constant impedance.

## 2. MODELING OF 3-PHASE DC/AC CONVERTER & COMPARISON TO SYNCHRONOUS MACHINE

### *2.1 Model of 3-Phase DC/AC Converter*

*Assumption 1.* (AC Signals). All 3-phase AC quantities $z = (z_a, z_b, z_c) \in \mathbb{R}^3$ are considered to be balanced: $z_a + z_b + z_c = 0$. We denote by $z_{\alpha\beta} \in \mathbb{R}^2$ the representation in $(\alpha\beta)$ domain, orthogonal to [1 1 1] and omit the third component, denoted by $z_\gamma \in \mathbb{R}$, see also Remark 3.

In this section, we consider an averaged model of a 3-phase converter composed of a linear DC circuit, a linear AC circuit and a nonlinear modulation block as depicted in Figure 1, see also the model in (Tabesh and Iravani, 2009).

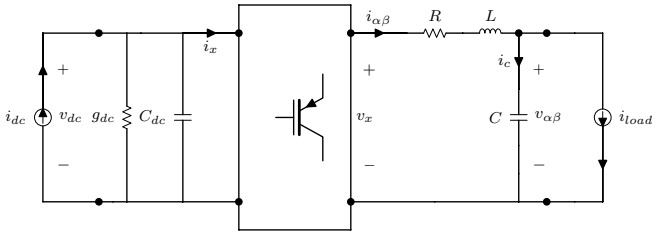


Fig. 1. Circuit diagram of a 3-phase DC/AC converter

- The DC input stage is represented by a constant current source $i_{dc} > 0$, in parallel to a capacitance $C_{dc} > 0$ and a conductance $G_{dc} > 0$; $i_x \in \mathbb{R}$ is the current at the output of the DC circuit and $v_{dc} \in \mathbb{R}$, the voltage across the DC capacitance. An interpretation of the DC source is that of a proportional control $u = G_{dc}\,(v_{dc,ref} - v_{dc})$ tracking the constant reference $v_{dc,ref} = i_{dc}/G_{dc}$ with $i_x$ as a disturbance input.

- The AC circuit contains at each phase an inductance $L > 0$ in series with a resistance $R > 0$ connected to a shunt capacitance $C > 0$ to ground. Here $v_{\alpha\beta} \in \mathbb{R}^2$ is the AC voltage across the capacitor, $i_{load} \in \mathbb{R}^2$ is the AC current drawn by the external load, $i_{\alpha\beta} \in \mathbb{R}^2$ is the AC current in the inductance and $v_x \in \mathbb{R}^2$ the average AC voltage at the switching node.

- The switching block represents an averaged model of a 6-switch 2-level inverter which modulates DC voltage into AC voltage according to a complementary switching pattern and a modulation signal $m_{\alpha\beta} \in \mathbb{R}^2$. For the time scale of interest, we assume a high enough switching frequency which allows us to discard all switching harmonics. This block represents the main nonlinearity in our system and is defined by the identities (Tabesh and Iravani, 2009):

$$i_x = \frac{1}{2} m_{\alpha\beta}^\top i_{\alpha\beta}\,, v_x = \frac{1}{2} m_{\alpha\beta} v_{dc}\,,$$

where $m_{\alpha\beta} \in \mathbb{R}^2$ as the modulation signal in $(\alpha\beta)$-frame, corresponding to the average of the converter duty cycle over one switching period and therefore its components take values in $[-1, 1]$. The modulation signal will serve as our main control input later on.

In summary, the 3-phase DC/AC converter model is

$$C_{dc}\dot{v}_{dc} = -G_{dc} v_{dc} + i_{dc} - \frac{1}{2} i_{\alpha\beta}^\top m_{\alpha\beta} \tag{1a}$$

$$C\dot{v}_{\alpha\beta} = -i_{load} + i_{\alpha\beta} \tag{1b}$$

$$L(\dot{i_{\alpha\beta}}) = -R i_{\alpha\beta} - v_{\alpha\beta} + \frac{1}{2} v_{dc} m_{\alpha\beta}\,, \tag{1c}$$

where all quantities in (1) are averaged over one switching cycle. We note that for modulation signal $m_{\alpha\beta}$ the system (1) is passive with respect to the AC grid port as well as the DC port. Passivity serves as a local stability certificate (van der Schaft, 1996; Fiaz et al., 2013) that allows to connect the converter to the AC grid or any DC source in a stable fashion provided that those are passive as well.

*Lemma 1.* (Modulation-independent passivity). Consider the DC/AC converter model (1). For any modulation signal $m_{\alpha\beta}$, this system is passive with respect to the input $u = \begin{bmatrix} i_{dc} & -i_{load}^\top \end{bmatrix}^\top$ and the output $y = \begin{bmatrix} v_{dc} & v_{\alpha\beta}^\top \end{bmatrix}^\top$.

**Proof.** Inspired by circuit theory, consider the positive definite storage function, $S : \mathbb{R}^5 \to \mathbb{R}_{\geq 0}$, defined as

$$S(v_{dc}, v_{\alpha\beta}, i_{\alpha\beta}) = \frac{1}{2} C_{dc} v_{dc}^2 + \frac{1}{2} C v_{\alpha\beta}^\top v_{\alpha\beta} + \frac{1}{2} L i_{\alpha\beta}^\top i_{\alpha\beta}\,. \tag{2}$$

We calculate the directional derivative of $S$ along the vector field (1) describing DC/AC converter dynamics as

$$\dot{S} = \begin{bmatrix} v_{dc} \\ v_{\alpha\beta} \\ i_{\alpha\beta} \end{bmatrix}^\top \begin{bmatrix} -G_{dc} & 0 & 0 \\ 0 & 0 & 0 \\ 0 & 0 & -RI_2 \end{bmatrix} \begin{bmatrix} v_{dc} \\ v_{\alpha\beta} \\ i_{\alpha\beta} \end{bmatrix} + \begin{bmatrix} i_{dc} & -i_{load} \end{bmatrix} \begin{bmatrix} v_{dc} \\ v_{\alpha\beta} \end{bmatrix},$$

where $I_2$ is the identity matrix in $\mathbb{R}^2$. The claim follows from the definition of passivity (van der Schaft, 1996). □

### *2.2 The Synchronous Machine Model*

The aim of this section is to highlight a particular structure of the SM model which lends itself useful in designing a matching controller for the 3-phase DC/AC converter. We consider a single-pole-pair, non-salient rotor, externally excited SM in $(\alpha\beta)$-frame as in (Caliskan and Tabuada, 2014), together with an output AC capacitor at the terminals, described by the following state space model:

$$\dot{\theta} = \omega \tag{3a}$$

$$M\dot{\omega} = -D\omega + \tau_m - \tau_e \tag{3b}$$

$$C\,\dot{v}_{\alpha\beta} = -i_{load} + i_{\alpha\beta} \tag{3c}$$

$$\dot{\lambda}_{\alpha\beta} = -R i_{\alpha\beta} - v_{\alpha\beta} \tag{3d}$$

Here $M > 0$ and $D > 0$ are the rotor inertia and damping coefficients, $\tau_m$ is the driving mechanical torque, and $\tau_e$ is the electrical torque. We denote the rotor angle by $\theta \in \mathbb{S}^1$, its angular velocity by $\omega \in \mathbb{R}$, the magnetic flux in the stator winding by $\lambda_{\alpha\beta} \in \mathbb{R}^2$, and the stator resistance by $R > 0$. At its terminals the machine is interfaced to the grid through a shunt capacitor with capacitance $C > 0$ and capacitor voltage $v_{\alpha\beta} \in \mathbb{R}^2$, and the terminal load current (exciting the machine) is denoted by $i_{load} \in \mathbb{R}^2$.

*Assumption 2.* (Regulated rotor field current). The rotor winding described by the magnetic flux $\lambda_f$, is omitted in our equations but it is considered as in (Caliskan and Tabuada, 2014) with the assumption that the rotor current $i_f$ is externally regulated to a constant value. □

We define the electromagnetic energy in the machine $W_e$ as

$$W_e = \begin{bmatrix}\lambda_{\alpha\beta}^\top & \lambda_f\end{bmatrix} L_\theta^{-1} \begin{bmatrix}\lambda_{\alpha\beta} \\ \lambda_f\end{bmatrix}, \tag{4}$$

where we made use of the inductance matrix $L_\theta$

$$L_\theta = \begin{bmatrix} L_s & 0 & L_m\cos(\theta) \\ 0 & L_s & L_m\sin(\theta) \\ L_m\cos(\theta) & L_m\sin(\theta) & L_f \end{bmatrix},$$

where $L_m > 0$ is the stator-to-rotor mutual inductance, $L_s > 0$ the stator inductance and $L_f > 0$ the winding field inductance. We obtain the following expressions the inductance current $i_{\alpha\beta} \in \mathbb{R}^2$

$$\begin{bmatrix} i_{\alpha\beta} \\ i_f \end{bmatrix} = \begin{bmatrix} \frac{\partial W_e}{\partial \lambda_{\alpha\beta}} \\ \frac{\partial W_e}{\partial \lambda_f} \end{bmatrix} = L_\theta^{-1} \begin{bmatrix} \lambda_{\alpha\beta} \\ \lambda_f \end{bmatrix}, \tag{5}$$

and for the electrical torque $\tau_e$

$$\tau_e = \frac{\partial W_e}{\partial \theta} = -i_{\alpha\beta}^\top L_m i_f \begin{bmatrix} -\sin(\theta) \\ \cos(\theta) \end{bmatrix}. \tag{6}$$

By using identity (5) in equation (3d), we express the stator dynamics in terms of current as:

$$L_s(\dot{i_{\alpha\beta}}) = -Ri_{\alpha\beta} - v_{\alpha\beta} - \dot\theta L_m i_f \begin{bmatrix} -\sin(\theta) \\ \cos(\theta) \end{bmatrix}. \tag{7}$$

We can identify the electromotive force (EMF) in the machine with the last term in (7). Hence, we rewrite (3) as

$$\dot\theta = \omega \tag{8a}$$

$$M\dot\omega = -D\omega + \tau_m + i_{\alpha\beta}^\top L_m i_f \begin{bmatrix} -\sin(\theta) \\ \cos(\theta) \end{bmatrix} \tag{8b}$$

$$C\dot v_{\alpha\beta} = -i_{load} + i_{\alpha\beta} \tag{8c}$$

$$L_s(\dot{i}_{\alpha\beta}) = -Ri_{\alpha\beta} - v_{\alpha\beta} - \omega L_m i_f \begin{bmatrix} -\sin(\theta) \\ \cos(\theta) \end{bmatrix} \tag{8d}$$

Observe the similarities between the converter model (1) and the SM model (8). The DC circuit is analogous to the rotor mass, and the electrical torque and EMF play a similar role as $i_x$ and $v_x$ in the converter model (1).

### *2.3 Synchronous Machine Matching Control*

In this section, we propose modulation controller to *match* the closed-loop dynamics of the converter (1) to the dynamics of a SM (8). Our design consists of two steps.

The first step in our design is to assign a sinusoidal modulation scheme according to the following map $m_{\alpha\beta} : \mathbb{S}^1 \to \mathbb{S}^1_\mu = \{x \in \mathbb{R}^2 : \|x\|_2 = \mu\}$, such that

$$\boxed{m_{\alpha\beta} = \mu \begin{bmatrix} -\sin(\theta_v) \\ \cos(\theta_v) \end{bmatrix}}, \tag{9}$$

where $\theta_v \in \mathbb{S}^1$ is an angle to be specified, while the gain $\mu \in ]0, 1]$ is constant and represents an amplitude for the modulation sinusoid.

The second step is to introduce the *virtual angle* $\theta_v$ resembling the SM rotor angle and assign to it the dynamics

$$\boxed{\dot\theta_v = \eta\, v_{dc}}, \tag{10}$$

where $\eta > 0$ is a constant gain to be specified. For example, a reasonable choice for $\eta$ would be the ratio between the nominal AC frequency and the DC voltage reference. By using (9), we can now write $i_x$ and $v_x$ as

$$i_x = \frac{1}{2} i_{\alpha\beta}^\top \mu \begin{bmatrix} -\sin(\theta_v) \\ \cos(\theta_v) \end{bmatrix}, \; v_x = \frac{1}{2} v_{dc}\, \mu \begin{bmatrix} -\sin(\theta_v) \\ \cos(\theta_v) \end{bmatrix}. \tag{11}$$

In the following we further highlight the similarities between the generator model (8) and the converter model (1) under the control scheme (9), (10). For this purpose, we identify the average switch voltage $v_x$ with a *virtual electromotive force* by defining the following relation:

$$\mu = -2\eta L_m i_f \tag{12}$$

By means of (6), (11) and (12), we identify the DC-side average switch current $i_x$ with the *virtual electrical torque*

$$\tau_{e,v} = \frac{1}{\eta} \cdot \frac{1}{2} i_{\alpha\beta}^\top \mu \begin{bmatrix} -\sin(\theta_v) \\ \cos(\theta_v) \end{bmatrix} = \frac{1}{\eta} i_x. \tag{13}$$

Next, we denote the *virtual angular velocity* by $\omega_v = \eta\, v_{dc}$ and rewrite the equivalent closed-loop converter model after dividing by $\eta^2$ to relate $\tau_{e,v}$, as in (13)

$$\dot\theta_v = \omega_v \tag{14a}$$

$$\frac{C_{dc}}{\eta^2}\dot\omega_v = -\frac{G_{dc}}{\eta^2}\omega_v + \frac{i_{dc}}{\eta} - \frac{1}{\eta} i_x \tag{14b}$$

$$C\dot v_{\alpha\beta} = -i_{load} + i_{\alpha\beta} \tag{14c}$$

$$L(\dot{i}_{\alpha\beta}) = -Ri_{\alpha\beta} - v_{\alpha\beta} + \frac{1}{2\eta}\omega_v m_{\alpha\beta}. \tag{14d}$$

By attributing proper units to $\eta$, we can now identify $C_{dc}/\eta^2$, $G_{dc}/\eta^2$, and $i_{dc}/\eta$ with the mechanical inertia damping factor, and driving torque of an equivalent SM.

*Remark 2.* (Matching vs virtual emulation). In the works of Bevrani et al. (2014); D'Arco and Suul (2013); Zhong and Weiss (2011); Vasileios Karapanos (2011) and references therein, the behavior of a SM is emulated in software (with virtual storage elements) which further provides setpoints for the inner loops of the converter control, for which a time-scale separation is assumed. Comparatively, since only the physical storage provided by the DC-link capacitor is involved, the size of the resulting inertia constant [1] is estimated to be roughly three orders of magnitude smaller than the inertia constant of a SM; see (Wittig et al., 2009) for a typical inverter design. Our controller (9)-(10) can be regarded as an *inner loop* that structurally equivalences a converter and a SM model. Based on this inner loop, further *outer loop controls* can be added by

[1] We define the inertia constants of the SM, respectively the converter, as the ratio between the nominal energy in the rotor mass, respectively in the DC-link capacitor, and rated apparent power.

modulating $i_{dc}$, $\eta$, and $\mu$, e.g., the equivalent of excitation or governor control to regulate frequencies and voltages, to tightly control currents, or to induce virtual inertia. □

*Remark 3.* (The $\gamma$-component). We now consider the $\gamma$-component of the converter AC signals. By construction of the modulation vector, we have $v_{x,\gamma} = 0$. For a balanced load, we have $i_{load,\gamma} = 0$. We are left with the following asymptotically stable dynamics for the $\gamma$-component:

$$L(\dot{i_\gamma}) = -Ri_\gamma - v_\gamma \tag{15a}$$
$$C\dot{v}_\gamma = i_\gamma \,. \tag{15b}$$

Since (15) is an asymptotically stable dynamical system, the omission of the $\gamma$-component is well justified. □

*Remark 4.* (Virtual and adaptive oscillator interpretation). By defining $\xi \in \mathbb{R}^2$ as a controller state, we can rewrite the controller (9)-(10) as the nonlinear feedback oscillator

$$\dot{\xi} = \eta\, v_{dc} \begin{bmatrix} 0 & 1 \\ -1 & 0 \end{bmatrix} \xi \;,\; m_{\alpha\beta} = -\mu\, \xi \tag{16}$$

where $\|\xi(0)\|_2 = 1$. As depicted in Figure 2, we can interpret the emulation control (9),(10) as an oscillator with constant amplitude $\|m(0)\|_2 = \mu$ and state-dependent frequency $\omega_v = \eta\, v_{dc}$ in feedback with the DC/AC converter dynamics (1). This control strategy structurally resembles the classic *proportional resonant control* (Teodorescu et al., 2006) with the difference that the frequency of the oscillator (16) actually adapts to the DC voltage which again reflects the grid state. Another related control strategy is *virtual oscillator control* encoding the inverter terminal dynamics as a nonlinear limit cycle oscillator adapting to the grid state (Johnson et al., 2014; Sinha et al., 2015). □

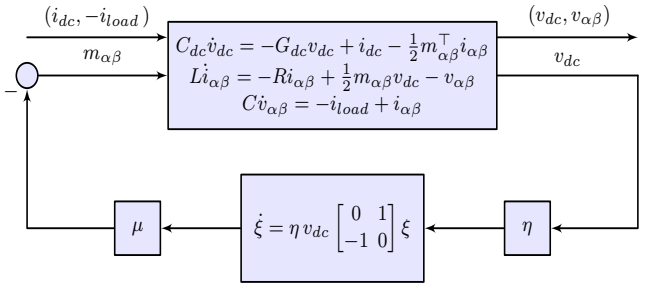


Fig. 2. Closed-loop system comprising the converter dynamics (1) and the controller dynamics (16).

## 3. PLUG-AND-PLAY PROPERTIES OF THE EMULATION CONTROLLER

For large-scale power network applications, key requirements for a *plug-and-play* operation (independent of the number and type of the devices connected to the grid) are decentralized stability and robustness certificates, e.g., by means of passivity (Fiaz et al., 2013), and power sharing amongst multiple inverters guaranteed by droop behavior (Dörfler et al., 2016) trading off active and reactive power injections with the voltage amplitude and frequency. In the following, we investigate these plug-and-play properties for the closed-loop system (1), (9), and (10).

### *3.1 Passivity of the Closed-Loop System*

We first note that the closed-loop dynamics (1), (9), (10) are passive as in Lemma 5 also when augmenting the storage function (2) with an additional term accounting for the dynamics of the matching controller (16). Consider the positive definite storage function $W : \mathbb{R}^7 \to \mathbb{R}_{\geq 0}$

$$W(v_{dc}, v_{\alpha\beta}, i_{\alpha\beta}, m_{\alpha\beta}) = S(v_{dc}, v_{\alpha\beta}, i_{\alpha\beta}) + \frac{1}{2} m_{\alpha\beta}^\top m_{\alpha\beta} \,,$$

where $S(v_{dc}, v_{\alpha\beta}, i_{\alpha\beta})$ is defined in (2). The derivative along trajectories of the closed loop (1), (16) is given by

$$\dot{W} = \dot{S} + m_{\alpha\beta}^\top \dot{m}_{\alpha\beta} \tag{17a}$$
$$= \dot{S} + \eta\, v_{dc}\, m_{\alpha\beta}^\top \begin{bmatrix} 0 & -1 \\ 1 & 0 \end{bmatrix} m_{\alpha\beta} \tag{17b}$$
$$\leq [i_{dc} \;\; -i_{load}] \begin{bmatrix} v_{dc} \\ v \end{bmatrix} \,. \tag{17c}$$

Hence the closed loop (1),(16) (and thus also (1), (9), (10)) is passive with input $(i_{dc}, -i_{load})$ and output $(v_{dc}, v_{\alpha\beta})$.

*Lemma 5.* (Closed-Loop Passivity). Consider the DC/AC converter model (1) with the modulation control (16). The closed-loop system (1),(16) is passive with respect to the input $u = \begin{bmatrix} i_{dc} & -i_{load}^\top \end{bmatrix}^\top$ and the output $y = \begin{bmatrix} v_{dc} & v_{\alpha\beta}^\top \end{bmatrix}^\top$.

An alternative storage function $H_v$ is the sum of $S$ in (2) and the electromagnetic energy $W_e$ stored in the field winding of the equivalent SM as in (4). As shown by Caliskan and Tabuada (2014), this storage function delivers the analogous passivity property. In our notation, $H_v$ is, up to potential energy $K_f$ due to constant excitation,

$$H_v = S + K_f + \frac{1}{2\eta} i_{\alpha\beta}^\top \begin{bmatrix} 0 & -1 \\ 1 & 0 \end{bmatrix} m_{\alpha\beta} \,. \tag{18}$$

### *3.2 Power Injection at the Output of the Modulation Block*

We now provide an investigation of the proposed controller by studying the steady-state AC power injection at the output of the modulation block. Accordingly, we introduce the following definitions as in (Gross et al., 2016):

*Definition 1.* (Steady-state of DC/ AC Signal). An AC signal $z_{\alpha\beta} \in \mathbb{R}^2$ is said to be in (synchronous and balanced) steady state, when it satisfies the following differential equation for some nonzero synchronous frequency $\omega_s \in \mathbb{R}$:

$$\dot{z}_{\alpha\beta} = \omega_s \begin{bmatrix} 0 & -1 \\ 1 & 0 \end{bmatrix} z_{\alpha\beta} \,.$$

Similarly, a DC signal $z_{dc} \in \mathbb{R}$ is said to be in steady-state when it satisfies the differential equation $\dot{z}_{dc} = 0$.

*Assumption 3.* (Feasibility). We assume that a non-trivial steady state exists for all DC and AC signals.

*Definition 2.* (Instantaneous AC Power). We define the active and reactive power flowing out of an AC voltage node $u_{\alpha\beta}$ on an edge defined by an AC current $y_{\alpha\beta}$ as

$$P_u = u_{\alpha\beta}^\top y_{\alpha\beta}$$
$$Q_u = u_{\alpha\beta}^\top \begin{bmatrix} 0 & -1 \\ 1 & 0 \end{bmatrix} y_{\alpha\beta} \,.$$

This definition is in accordance with Akagi's instantaneous power theory (Hirofumi Akagi and Nabae, 1983).

*Theorem 6.* (Active And Reactive Power). Consider the converter model (1) together with the controller (9), (10). Assume that all DC and AC signals are in steady state as described in Definition 1 with synchronous frequency $\omega_s$. Let $P_x$ denote the active power flowing out of the

average switching voltage node $v_x$ and let $r_x$ and $\omega_x$ be its amplitude and frequency, then the following holds:

$$r_x = \frac{\mu}{4G_{dc}}(i_{dc} \pm \sqrt{i_{dc}^2 - 4G_{dc}P_x}) \tag{20a}$$

$$\omega_x = \frac{\eta}{2G_{dc}}(i_{dc} \pm \sqrt{i_{dc}^2 - 4G_{dc}P_x}), \tag{20b}$$

with $\omega_x = \omega_s$ by assumption. Moreover, there is no influence of reactive power $Q_x$ on the amplitude and frequency $(r_x, \omega_x)$.

**Proof.** Consider the dynamics of DC circuit as described in (1a) at steady state, i.e, when $\dot{v}_{dc} = 0$:

$$0 = -G_{dc}v_{dc} + i_{dc} - i_x\,. \tag{21}$$

The active power at the switching node is given by

$$P_x = v_x^\top i_{\alpha\beta} = \frac{1}{2}m_{\alpha\beta}^\top v_{dc} i_{\alpha\beta} = i_x v_{dc}\,.$$

We multiply (21) by $v_{dc}$ to obtain quadratic expression relating $P_x$ and $v_{dc}$ at steady state.

$$v_{dc} = \frac{i_{dc} \pm \sqrt{i_{dc}^2 - 4G_{dc}P_x}}{2G_{dc}}\,. \tag{22}$$

Note that the amplitude $r_x$ and frequency $\omega_x$ at the switching node can be expressed as

$$r_x = \frac{1}{2}\mu\, v_{dc},\ \omega_x = \eta\, v_{dc}\,. \tag{23}$$

We have that (20) follows directly from (22) and (23). □

Due to positivity of the amplitude $r_x > 0$ and the frequency $\omega_x > 0$, only the positive solutions of (20) are practically relevant for the forthcoming analysis. Equations (20) relate the active power $P_x$ flowing out from the switching node and the amplitude $r_x$ and frequency $\omega_x$ of the switching node voltage at steady state.

In the following, we characterize the voltage and frequency droop slopes [2] induced by our emulation controller (9), (10) at a particular steady state of the switching voltage $v_x$ written in terms of its amplitude $r_x$ and frequency $\omega_x$.

*Corollary 7.* (Droop Coefficients). Around a steady-state operating point $(r_x, \omega_x)$, the following active power droop coefficients are found:

$$d_{r_x} = -\frac{8G_{dc}}{\mu^2}r_x + \frac{2i_{dc}}{\mu}\ ,\ d_{\omega_x} = -\frac{2G_{dc}}{\eta^2}\omega_x + \frac{i_{dc}}{\eta}\,. \tag{24}$$

**Proof.** From equations (20), the active power $P_x$ expression at steady state can be given as a function of $r_x$ and $\omega_x$

$$P_x = \frac{-4G_{dc}}{\mu^2}r_x^2 + \frac{2i_{dc}}{\mu}r_x = \frac{-G_{dc}}{\eta^2}\omega_x^2 + \frac{i_{dc}}{\eta}\omega_x\,. \tag{25}$$

By linearizing equation (25) around the operating point $(r_x, \omega_x)$, we find the droop slopes in (24). □

Corollary 7 suggests that, when using $i_{dc}$ in an outer loop for frequency or voltage regulation, then the droop slopes are inversely proportional to $\mu$ and $\eta$, respectively.

*Corollary 8.* (Maximal active power). The maximal active power $\bar{P}_x$ that can be delivered at the switching node is

$$\bar{P}_x = \frac{i_{dc}^2}{4G_{dc}}\,.$$

[2] Here, the droop slopes $d_{r_x}$ and $d_{\omega_x}$ describe the locally linear sensitivity relating the active power injection $P_x$ at the switching node and its steady-state voltage amplitude $r_x$ and frequency $\omega_x$.

**Proof.** The maximum $\bar{P}_x$ of the parabolic equation (25) describing $P_x$ is attained when $dP_x/dr_x = 0$ or $dP_x/d\omega_x = 0$. Equivalently, we obtain

$$\bar{P}_x = \frac{-4G_{dc}}{\mu^2}\bar{r}_x^2 + \frac{2i_{dc}}{\mu}\bar{r}_x = \frac{i_{dc}^2}{4G_{dc}}\,,$$

where $\bar{r}_x = \mu i_{dc}/4G_{dc}$ is the maximal amplitude and $\bar{\omega}_x = \eta i_{dc}/2G_{dc}$ is the maximal frequency. □

The maximal deliverable AC active power is naturally constrained by the maximal DC power in accordance with the maximum power transfer theorem (William H. Hayt Jr., 2012).

*Remark 9.* (Steady-state power balance at the filter node). We assume all AC quantities are synchronized at the same frequency $\omega_s$ at steady state. In this case, the active and reactive power $P_{load}\,, Q_{load}$ at the at the filter node (i.e., after the converter output filter) is described as:

$$\begin{bmatrix} P_{load} \\ Q_{load} \end{bmatrix} = \begin{bmatrix} P_x \\ Q_x \end{bmatrix} + \begin{bmatrix} -Rr_L^2 \\ \omega_s L r_L^2 + \omega_s C r_C^2 \end{bmatrix}\,,$$

with $r_L$ as the amplitude of $i_{\alpha\beta}$ and $r_C$ as the amplitude of $v_{\alpha\beta}$. This relation describes the apparent power balance in the converter at steady state. □

## 4. CASE STUDY

For the following simulation case study, we consider a converter rated in the 10 KW range, with the choice of parameters, in S.I. units as: $i_{dc} = 100, G_{dc} = 0.1, C_{dc} = 0.001$, $R = 0.1$, $L = 5 \cdot 10^{-4}$, $C = 10^{-5}$, and nominal [3] DC voltage of $v_{dc,ref} = 1000$. In order to obtain the desired nominal values in (S.I) $r_{x,ref} = 165$ and $\omega_{x,ref} = 2\pi 50$, we choose the controller gains as:

$$\eta = \frac{\omega_{x,ref}}{v_{dc,ref}} = 0.3142,\ \mu = \frac{2r_{x,ref}}{v_{dc,ref}} = 0.33\,.$$

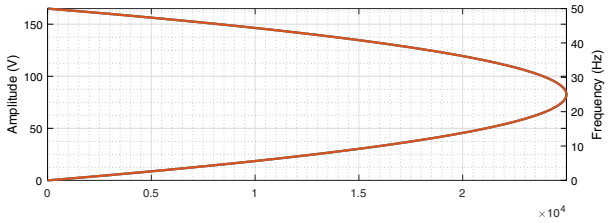


Fig. 3. Steady-state $(r_x, P_x)$ and $(\omega_x, P_x)$ profiles as in (20)

In Figure 3, the analytical solution found in (20) is plotted for the current choice of parameters. A magnified version of

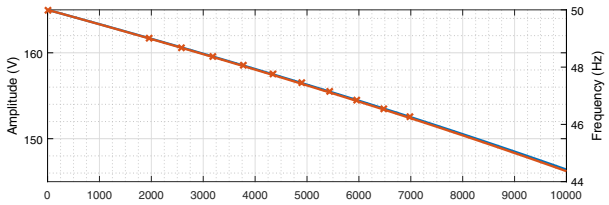


Fig. 4. Analytical plot overlaid with simulated operating points for $r_x$ and $\omega_x$ versus $P_x$

[3] We refer DC and AC quantities as *nominal* when they are in the steady-state induced by an open-circuit operation with $i_{load} = 0$.

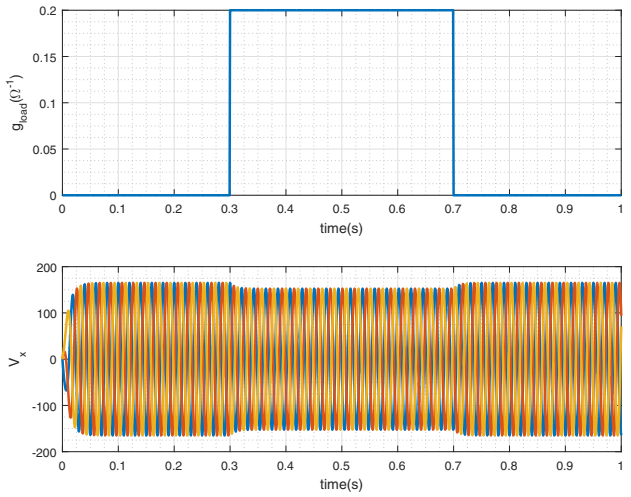


(a) Resistive load profile and voltage $v_x$

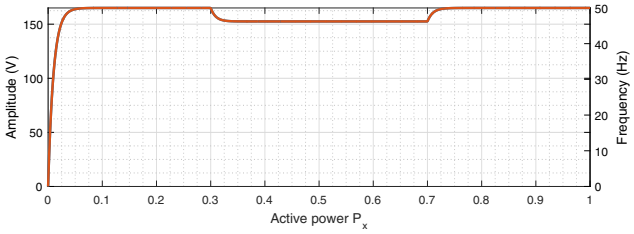


(b) Amplitude and Frequency of $v_x$

Fig. 5. Time-domain simulation of the closed loop converter model interfaced with a resistive load.

Figure 3, near the nominal, is shown in Figure 4, where the analytic curves (20) are overlaid with steady-state values from numerical experiments. Observe the nearly linear droop characteristics at the operating points.

We then run time-domain simulations for the initial condition $v_{dc}(0) = 0$ and with a time-varying and balanced load profile undergoing step changes starting from $t_s = 0.3s$ in the load conductance (Figures 5). Notice the initial charging of the DC capacitor and the dependency of the amplitude and frequency on the active power which match our analytic and numeric results in (20) and in Figure 4.

## 5. CONCLUSIONS

We proposed a novel converter control strategy that is motivated by the similarities between the rotor dynamics of a synchronous machine and the DC-link storage present in a converter. Our controller matches these two models, induces droop properties, and preserves passivity characteristics of the converter. Simulation results confirm the predicted behavior. Our control strategy involves adding only a single integrator and requires only readily available DC-side measurements. It can also be regarded as an inner loop that induces a limit-cycle oscillator behavior. Based on this inner loop, further outer loop controls can be constructed, e.g., the equivalent of excitation or governor control, to provide reactive power, or to regulate currents and voltages within limits. Important aspects of further analysis of the proposed controller are stable power sharing and frequency regulation in a multiple-converter system.

## REFERENCES


Arani, M.F. and El-Saadany, E.F. (2013). Implementing virtual inertia in dfig-based wind power generation. *Power Systems, IEEE Transactions on*, 28(2), 1373–1384.

Bevrani, H., Ise, T., and Miura, Y. (2014). Virtual synchronous generators: A survey and new perspectives. *International Journal of Electrical Power and Energy Systems*, 54(C), 244–254.

Caliskan, S.Y. and Tabuada, P. (2014). Compositional transient stability analysis of multimachine power networks. *Control of Network Systems, IEEE Transactions on*, 1(1), 4–14.

D'Arco, S. and Suul, J.A. (2013). Virtual synchronous machines—Classification of implementations and analysis of equivalence to droop controllers for microgrids. *PowerTech (POWERTECH)*.

Denis, G., Prevost, T., Panciatici, P., Kestelyn, X., Colas, F., and Guillaud, X. (2015). Review on potential strategies for transmission grid operations based on power electronics interfaced voltage sources.

Dörfler, F., Simpson-Porco, J.W., and Bullo, F. (2016). Breaking the Hierarchy: Distributed Control & Economic Optimality in Microgrids. *IEEE Transactions on Control of Network Systems*. URL `http://arxiv.org/abs/1401.1767`.

ENTSOE, R.C.S.P..D.S.G. (2016). Frequency stability evaluation criteria for the synchronous zone of continental europe. Technical report.

Fiaz, S., Zonetti, D., Ortega, R., Scherpen, J., and van der Schaft, A. (2013). A port-hamiltonian approach to power network modeling and analysis. *European Journal of Control*, 19(6), 477 – 485.

Gross, D., Arghir, C., and Dörfler, F. (2016). On the steady-state behavior of a nonlinear power system model. URL `https://arxiv.org/abs/1607.01575`. Submitted. Available at `https://arxiv.org/abs/1607.01575`.

Hirofumi Akagi, Yoshihira Kanazawa, K.F. and Nabae, A. (1983). Generalized theory of instantaneous reactive power and its application.

Johnson, B., Dhople, S., Hamadeh, A., and Krein, P. (2014). Synchronization of nonlinear oscillators in an lti electrical power network. *Circuits and Systems I: Regular Papers, IEEE Transactions on*, 61(3), 834–844.

M.P.N van Wesenbeeck, S.W.H. de Haan, P.V. and Visscher, K. (2009). Grid tied converter with virtual kinetic storage.

Sinha, M., Dörfler, F., Johnson, B., and Dhople, S. (2015). Uncovering droop control laws embedded within the nonlinear dynamics of Van der Pol oscillators. *IEEE Transactions on Control of Network Systems*. URL `http://arxiv.org/abs/1411.6973`.

Tabesh, A. and Iravani, R. (2009). Multivariable dynamic model and robust control of a voltage-source converter for power system applications. *Transactions on power delivery, IEEE*, 24(1).

Teodorescu, R., Blaabjerg, F., Liserre, M., and Loh, P.C. (2006). Proportional-resonant controllers and filters for grid-connected voltage-source converters. *IEE Proceedings Electric Power Applications*, 153(5), 750–762.

Tielens, P. and Van Hertem, D. (2016). Renewable and Sustainable Energy Reviews. *Renewable and Sustainable Energy Reviews*, 55(C), 999–1009.

van der Schaft, A.J. (1996). *L2-Gain and Passivity Techniques in Nonlinear Control*, volume 218 of *Lecture Notes in Control and Information Sciences*.

Vasileios Karapanos, S.d.H.K.Z. (2011). Real Time Simulation of a Power System with VSG Hardware in the Loop. 1–7.

William H. Hayt Jr., Jack E. Kemmerly, S.M.D. (2012). *Engineering circuit analysis, Eighth Edition*. McGraw-Hill, New York.

Wittig, B., Franke, W.T., and Fuchs, F.W. (2009). Design and analysis of a dc/dc/ac three phase solar converter with minimized dc link capacitance. In *Power Electronics and Applications, 2009. EPE '09. 13th European Conference on*, 1–9.

Yong Chen, Ralf Hesse, D.T. and Beck, H.P. (2011). In *Improving the Grid Power Quality Using Virtual Synchronous Machines*.

Zhong, Q.C. and Weiss, G. (2011). Synchronverters: Inverters that mimic synchronous generators. 58(4), 1259–1267.